

A Statistical Reduced Complexity Climate Model for Probabilistic Analyses and Projections

Mikkel Bennedsen*, Eric Hillebrand†, Siem Jan Koopman‡

July 8, 2024

Abstract

We propose a new statistical reduced complexity climate model. The centerpiece of the model consists of a set of physical equations for the global climate system which we show how to cast in non-linear state space form. The parameters in the model are estimated using the method of maximum likelihood with the likelihood function being evaluated by the extended Kalman filter. Our statistical framework is based on well-established methodology and is computationally feasible. In an empirical analysis, we estimate the parameters for a data set comprising the period 1959–2022. A likelihood ratio test sheds light on the most appropriate equation for converting the level of atmospheric concentration of carbon dioxide into radiative forcing. Using the estimated model, and different future paths of greenhouse gas emissions, we project global mean surface temperature until the year 2100. Our results illustrate the potential of combining statistical modelling with physical insights to arrive at rigorous statistical analyses of the climate system.

*Department of Economics and Business Economics and CoRE, Aarhus University, Fuglesangs Allé 4, 8210 Aarhus V, Denmark. E-mail: mbennedsen@econ.au.dk

†Department of Economics and Business Economics and CoRE, Aarhus University, Fuglesangs Allé 4, 8210 Aarhus V, Denmark. E-mail: ehillebrand@econ.au.dk

‡Department of Econometrics, School of Business and Economics, Vrije Universiteit Amsterdam, De Boelelaan 1105, 1081 HV Amsterdam, The Netherlands, E-mail: s.j.koopman@vu.nl

1 Introduction

Climate models play an important role in our understanding of the past, present, and future climate. Most notably, the reports on the “physical science basis” for global warming, compiled by the Intergovernmental Panel on Climate Change (IPCC), rely heavily on output from large-scale Earth system models (Solomon et al., 2007; Stocker and Qin, 2013; Masson-Delmotte and Zhai, 2021). However, since these large-scale models require enormous amounts of computer power to run even a single instance, they are not suited for creating large ensembles of climate system variables, which could be useful for, e.g., probabilistic analysis and/or for studying the effects of a large number of different scenarios for future greenhouse gas emissions. In contrast to large-scale Earth system models, reduced complexity climate models (RCMs) are simpler climate models designed to run on desktop computers. The lower computational requirements of RCMs make them eminently suitable for running large ensembles and investigating the impact of a wide range of different greenhouse gas scenarios, as well as for probabilistic analysis, which would be infeasible using large scale models (Nicholls et al., 2020, 2021). RCMs are by now recognized as important tools for understanding the climate system. For instance, the “MAGICC” RCM (Meinshausen et al., 2011) is instrumental in probabilistic analyses of the climate system (Meinshausen et al., 2009) as well as in the construction of the influential Representative Concentration Pathway (RCP) scenarios (Meinshausen et al., 2011). Both MAGICC and the “FaIR” RCM (Leach et al., 2021) are extensively used in the 6th assessment report from the IPCC (AR6; Masson-Delmotte and Zhai, 2021, see, e.g., Chapter 7).

We consider a statistically-based RCM where the entire chain from emissions to temperatures is formulated as a statistical model with stochastic representations of variables and their dependencies implied by the underlying physics. This approach is in contrast to a physically-based RCM which is formulated as a deterministic model using equations reflecting the underlying physics. As a consequence, physically-based RCMs are not accounting for stochastic variation and uncertainty in the modeling framework, and hence the statistical properties of the calibrated/estimated model parameters are unknown. Furthermore, the informative and insightful “probabilistic” projections are not necessarily based on justified statistical foundations. Most RCMs that model the entire chain from emissions to temperatures are physically-based (Smith et al., 2024).¹

¹Notably, the most recent version of the FaIR model (Smith et al., 2024) treats the energy balance module statistically using the framework suggested in Cummins et al. (2020) and the remaining modules deterministically, putting this model somewhere in-between being statistically-based and physically-based.

In this paper, we propose and develop a fully statistical reduced complexity climate model (Stat-RCM) that models the entire chain from emissions to temperatures. We assume that the climate system consists of various latent processes — such as the atmospheric concentration of carbon dioxide (CO_2) and the mean temperature at the Earth’s surface — and that historical data are noisy observations of these variables. This framework allows us to cast the climate model in a state space system, where the state equations represent the latent “true” climate processes and the measurement equations express observations as noisy measurements of these latent processes. We then specify the transition equations of the state variables using functional forms which are chosen to be compatible with the physics underlying the climate system. The stochastic error processes in the state equation represent the difference between the latent “true” climate system and our functional representation of it.

Our proposed Stat-RCM treats the physical processes of the climate system at a lower resolution compared to physically-based RCMs, such as MAGICC (Meinshausen et al., 2011), FaIR (Leach et al., 2021), and Hector (Hartin et al., 2015). The simpler physical representation of the climate system employed by the Stat-RCM is necessitated by statistical identification, i.e., the condition that the objective function, usually the log-likelihood, as a function of the parameters of the model has a unique extremum. Identification allows for the invocation of standard statistical results, such as a law of large numbers and a central limit theorem. The former ensures that the estimator of the parameter vector is consistent and the latter ensures that the estimator is asymptotically normally distributed, which allows for assessment of parameter uncertainty. We use our framework in this study to (i) estimate the parameter vector of the model via the maximum likelihood method using historical data from the period 1959–2022; (ii) obtain standard errors for the estimated parameters; (iii) investigate the finite sample properties of the estimation method via Monte Carlo simulations; (iv) conduct model selection on the parts of the model that are not informed by physical first-principles; (v) extract estimates of the underlying “true” climate state variables; (vi) perform statistical validation of the model by showing that it can simulate climate variables that are compatible with the historical data record; and (vii) construct probabilistic projections of the climate system, conditional on a scenario for future greenhouse gas emissions. Our results illustrate the potential for combining statistical modelling with physical insight to arrive at rigorous probabilistic and statistical analyses of the climate system.

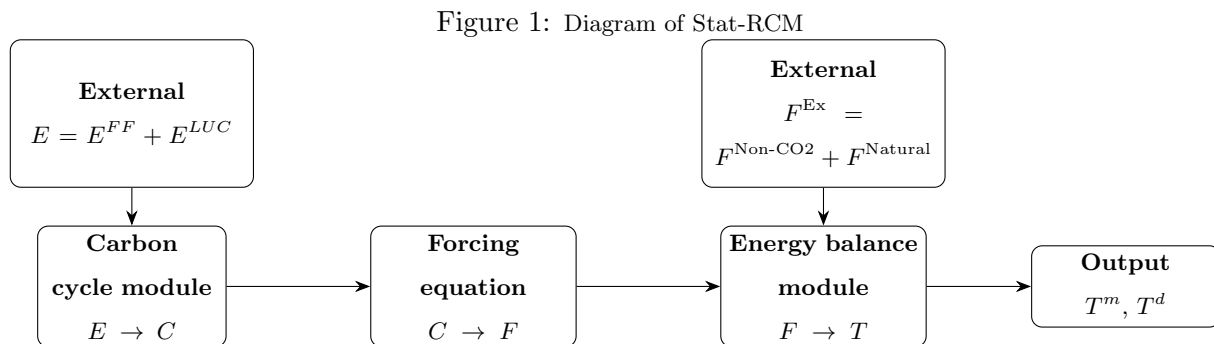
The remainder of the paper is structured as follows. In Section 2, we formulate the basic model equations of the Stat-RCM, and in Section 3 we show how to cast these equations into a non-linear

state space system. Section 4 presents the results from a Monte Carlo simulation study that aims to investigate the finite sample properties of the proposed estimation procedure. Section 5 shows and discusses the estimation results for the Stat-RCM based on historical data from the period 1959–2022. In Section 6 we adopt these estimation results and use these to generate projections of the future climate, conditional on given paths of greenhouse gases and other forcing agents. Section 7 concludes. An appendix contains supplementary empirical results and details on the implementation of the employed state space methods.

2 Stat-RCM: A new statistical reduced complexity climate model

An overview of Stat-RCM is given in Figure 1. The figure shows how anthropogenic CO₂ emissions from fossil fuels (E^{FF}) and land–use change (E^{LUC}) are affecting temperatures: first, total CO₂ emissions ($E = E^{FF} + E^{LUC}$) are converted into atmospheric concentrations (C) in a carbon cycle module; then atmospheric concentrations are converted into radiative forcing (F) using a forcing equation; lastly, an energy balance module converts radiative forcing into changes in surface temperature (T^m) and deep ocean temperature (T^d). CO₂ emissions and the forcing effects of non-CO₂ greenhouse gases ($F^{Non-CO2}$) and various natural phenomena such as volcanic eruptions and solar activity (F^{Nat}) are incorporated into the model as covariates, i.e. these processes are “external” and not determined inside the model.

The following subsections give further details on the three main modules in Stat-RCM, namely the carbon cycle module, the forcing equation, and the energy balance module. Similar models for the carbon cycle and energy balance modules were considered separately in Bennedsen et al. (2023) and Bennedsen et al. (2023), respectively. The Stat-RCM extends these models by connecting them through the forcing equation, thereby modelling the entire chain from emissions to temperatures, and by introducing climate feedbacks into the carbon cycle module.



2.1 Carbon cycle module

The cornerstone of the carbon cycle module is the carbon budget equation,

$$\frac{dC_t}{dt} = E_t^{FF} + E_t^{LUC} - S_t^{LND} - S_t^{OCN}, \quad (2.1)$$

where C_t is atmospheric concentration of carbon dioxide (CO₂) at time t , while E_t^{FF} and E_t^{LUC} are emissions of CO₂ at time t from fossil fuel burning and land-use change, respectively, and, S_t^{OCN} and S_t^{LND} are fluxes in the ocean and terrestrial (land) sink, respectively. Atmospheric concentrations, C_t , are given in gigatonnes of carbon (GtC), while all terms on the right hand side of Equation (2.1) are given in GtC *per year*. The carbon budget equation (2.1) captures the principle that Earth’s carbon cycle is ‘closed’ in the sense that all CO₂ emitted from human activities ($E_t^{FF} + E_t^{LUC}$) must be absorbed by one of the three carbon sinks, namely the atmosphere (dC_t/dt), the terrestrial biosphere (S_t^{LND}), and the oceanic biosphere (S_t^{OCN}); see [Friedlingstein et al. \(2022\)](#) for an extensive discussion of the carbon budget.

The emissions time series E_t^{FF} and E_t^{LUC} are considered as covariates (exogenous data), which “force” the carbon system. The stock time series C_t as well as the flux time series data S_t^{LND} and S_t^{OCN} are included as part of the dynamic model system and interact with the other variables in the model. As is common in reduced-form modelling of the carbon cycle, we will assume that the land and ocean fluxes are related to the level of atmospheric concentrations (C) and the state of the climate, represented by the global surface temperature above pre-industrial levels (T^m). In particular, we specify the dynamics of the sinks as

$$\begin{aligned} S_t^{OCN} &= g_{OCN}(C_t, T_t^m) - g_{OCN}(C_{1750}, T_{1750}^m) + \eta_t^O, \\ S_t^{LND} &= g_{LND}(C_t, T_t^m) - g_{LND}(C_{1750}, T_{1750}^m) + \eta_t^L, \end{aligned}$$

for non-linear functions $g_{OCN}(\cdot, \cdot)$ and $g_{LND}(\cdot, \cdot)$, and where the terms η_t^O and η_t^L are zero-mean stochastic processes, C_{1750} and T_{1750}^m denote the pre-industrial values of C and T^m , respectively, with default values given by $C_{1750} = 591.3060$ GtC and $T_{1750}^m = 0^\circ\text{C}$. The terms $g_i(C_{1750}, T_{1750}^m)$, for $i = OCN, LND$, are introduced to capture the assumption that the climate system was in equilibrium in the pre-industrial era, meaning that the net flux of CO₂ between the atmosphere and the sinks were zero on average, i.e. $\mathbb{E}[S_{1750}^{OCN}] = \mathbb{E}[S_{1750}^{LND}] = 0$, where $\mathbb{E}[\cdot]$ denotes the expectation operator.

Different RCMs consider different functional forms for g_{OCN} and g_{LND} . Over the time period studied in the empirical section below (1959–2022), the functions g_{OCN} and g_{LND} can be taken

to be approximately linear in concentrations C (Benedsen et al., 2023). We follow the MAGICC RCM (Meinshausen et al., 2011) approach and incorporate T^m via exponential functions,

$$\begin{aligned} g_{OCN}(C_t, T_t^m) &= b_1 C_t \exp(-c_1 T_t^m), \\ g_{LND}(C_t, T_t^m) &= b_2 C_t \exp(-c_2 T_t^m), \end{aligned}$$

where $b_1, b_2, c_1, c_2 \in \mathbb{R}$ are constant parameters. For $b_1, b_2 > 0$, the activity of the sinks depends positively on the level of atmospheric concentrations C , and we provide evidence of this below. For the land sink, this is due to the fertilization effect (e.g. Bacastow and Keeling, 1979), while for the ocean sink it is due to the fact that the uptake depends on the difference in partial pressure of CO_2 between the atmosphere and the upper ocean (e.g. Joos et al., 1996). The dependence of the sink uptake on the level of CO_2 concentrations in the atmosphere, is often referred to as the ‘carbon cycle feedback’. Conversely, the dependence of the sink uptakes on the state of the climate, represented by the global surface temperature T^m , is referred to as the ‘climate feedback’ (e.g. Friedlingstein et al., 2003; Fung et al., 2005; Friedlingstein, 2015).

2.2 Forcing equation

The forcing equation connects the level of CO_2 concentrations (given in GtC) to radiative forcing from CO_2 (given in W/m^2) above the pre-industrial level. Here, it is specified as

$$F_t^{CO_2} = g_F(C_t) - g_F(C_{1750}) + \eta_t^F, \quad (2.2)$$

where $g_F(\cdot)$ is a non-linear function describing the link between CO_2 concentrations and forcing, η_t^F is a zero-mean stochastic process, and the term $g_F(C_{1750})$ is introduced to reflect the assumption that the climate system was in equilibrium in the pre-industrial era, i.e. $\mathbb{E}[F_{1750}^{CO_2}] = 0$. In this study, we consider the following functional form for $g_F()$

$$g_F(C_t) = f_1 \log(C_t + f_2 C_t^2) + f_3 \sqrt{C_t}, \quad (2.3)$$

where $f_1, f_2, f_3 \in \mathbb{R}$ are unknown constant parameters. This specification for $g_F()$ is general and it nests several functional forms which have been used in the RCM literature previously. Setting $f_1 = f_2 = 0$ will result in the specification used in MAGICC6 (Meinshausen et al., 2011); setting $f_2 = 0$ will result in the specification used in FAIR (Leach et al., 2021); while $f_3 = 0$ yields the form proposed in Hansen et al. (1998). Below, we will exploit the statistical nature of the model to test which of these functional forms are most appropriate when confronted with historical data.

2.3 Energy balance module

For the energy balance module, we consider a two-box energy balance model (Gregory, 2000)

$$\begin{aligned} H_m \frac{dT_t^m}{dt} &= F_t - \lambda T_t^m - \gamma(T_t^m - T_t^d), \\ H_d \frac{dT_t^d}{dt} &= \gamma(T_t^m - T_t^d), \end{aligned}$$

where H_m and H_d are fixed unknown coefficients, T_t^m and T_t^d are time- t temperature anomalies (with respect to the pre-industrial period) in the atmosphere upper-ocean mixed layer and the deep ocean layer, respectively, F_t is time- t radiative forcing, and λ and γ are fixed unknown coefficients. The term $F_t = F_t^{CO_2} + F_t^{Ex}$ is the total radiative forcing in the system which we model as the sum of the forcing from CO₂ ($F_t^{CO_2}$ is modelled within the dynamic system) and forcing from other sources (F_t^{Ex} represents a set of covariates). The parameters H_m and H_d (given in $W \text{ year } m^{-2}K^{-1}$) are the corresponding heat capacities for the two layers, λ (given in $W \text{ m}^{-2}K^{-1}$) is a climate feedback parameter, and γ (given in $W \text{ m}^{-2}K^{-1}$) is the coefficient of heat exchange between the two layers.

In this study, we work with the two-box energy balance model as described above. However, it is straightforward to expand our setting to a general model with one box or multiple boxes. For instance, a three-box energy balance model can be considered using related methods to those considered in Cummins et al. (2020).

3 Non-linear state space representation of Stat-RCM

In this section, we show how to cast the climate model presented in Section 2 in a non-linear state space system. We do this by using an Euler discretization of the relevant continuous-time equations. A state space system consists of two sets of equations: (i) state equations for the latent system dynamic variables, and (ii) measurement equations for the observed data variables. In Section 3.1, we present the state equations which are obtained from the physical equations above. In Section 3.2, we present the measurement equations which specify the data observations as noisy measurements of the latent system variables. In Section 3.3, we collect the state and measurement equations into a state space system, which can then be estimated and analyzed using statistical methods designed for such systems. We refer to Durbin and Koopman (2012) for a textbook treatment on the statistical analysis of state space systems.

In what follows, let $\Delta > 0$ denote the length of a time step. In our applications of the model presented below, we will set $\Delta = 1$ year, but, for generality, we specify the model for a generic time step.

3.1 State equations

The carbon cycle module equations are discussed in Section 2.1 and, after some substitutions and minor manipulations, we have

$$\begin{aligned} C_{t+\Delta} &= C_t + (E_{t+\Delta} - S_{t+\Delta}^{LND} - S_{t+\Delta}^{OCN})\Delta, & S_{t+\Delta}^{OCN} &= -b_1 C_{1750} + b_1 C_t \exp(-c_1 T_t^d) + \eta_{t+\Delta}^O, \\ & & S_{t+\Delta}^{LND} &= -b_2 C_{1750} + b_2 C_t \exp(-c_2 T_t^d) + \eta_{t+\Delta}^L, \end{aligned}$$

where $b_1, b_2, c_1, c_2 \in \mathbb{R}$ are fixed unknown coefficients, $C_{1750} = 591.3060$ GtC is the pre-industrial level of CO₂ concentrations, $E_t = E_t^{FF} + E_t^{LUC}$, and disturbances $\eta_{t+\Delta}^O$ and $\eta_{t+\Delta}^L$ are mean-zero innovation terms. The forcing equation is discussed in Section 2.2 and we consider the equations (2.2)–(2.3) as given by

$$F_{t+\Delta}^{CO2} = g_F(C_t) - g_F(C_{1750}) + \eta_{t+\Delta}^F, \quad g_F(C_t) = f_1 \log(C_t + f_2 C_t^2) + f_3 \sqrt{C_t},$$

with mean-zero innovation $\eta_{t+\Delta}^F$ and $f_1, f_2, f_3 \in \mathbb{R}$ are fixed unknown coefficients. The energy balance module equations are discussed in Section 2.3 and are given by

$$\begin{aligned} T_{t+\Delta}^m &= \left(1 - \frac{\gamma + \lambda}{H_m} \Delta\right) T_t^m + \frac{\gamma \Delta}{H_m} T_t^d + \frac{\Delta}{H_m} (F_t^{CO2} + F_t^{Ex}) + \eta_{t+\Delta}^m, \\ T_{t+\Delta}^d &= \frac{\gamma \Delta}{H_d} T_t^m + \left(1 - \frac{\gamma \Delta}{H_d}\right) T_t^d + \eta_{t+\Delta}^d, \end{aligned}$$

where $\gamma, \lambda, H_m, H_d \in \mathbb{R}$ are fixed unknown coefficients, $F_t^{Ex} = F_t^{Non-CO2} + F_t^{Nat}$ is forcing from non-CO₂ sources (anthropogenic and natural), which are treated here as covariates, and disturbances $\eta_{t+\Delta}^m$ and $\eta_{t+\Delta}^d$ are mean-zero innovation terms.

3.2 Measurement equations

We assume that we have a number of observed variables available that we can regard as, possibly noisy, measurements for the state variables. We will denote most of these observed variables by the same name as their state variable counterparts but we affix an asterisk to it. Many different observed variables can be considered and the core selection typically depend on data availability. In our study, we consider the following set of seven observed variables with associated equations,

$$C_t^* = \mu_C + C_t + \epsilon_t^C, \quad (\text{CO2 concentrations})$$

$$\begin{aligned}
S_t^{OCN,*} &= \mu_O + S_t^{OCN} + \epsilon_t^{OCN}, & (\text{CO2 ocean sink}) \\
S_t^{LND,*} &= \mu_L + S_t^{LND} + \epsilon_t^{LND}, & (\text{CO2 land sink}) \\
F_t^{CO2,*} &= \mu_F + F_t^{CO2} + \epsilon_t^F, & (\text{Forcing from CO2}) \\
T_t^{m,*} &= \mu_m + T_t^m + \epsilon_t^m, & (\text{Surface temperature}) \\
T_t^{d,*} &= \mu_d + T_t^d + \epsilon_t^d, & (\text{Deep ocean temperature 0-2000m}) \\
O_t^* &= H_d \cdot \mu_d + H_d \cdot T_t^d + \epsilon_t^O, & (\text{Ocean heat content 0-2000m})
\end{aligned}$$

where H_d is the fixed unknown coefficient from the T_t^d state equation in Section 3.1, all ϵ_t variables are mean-zero error processes and the unknown fixed constants $\mu \in \mathbb{R}$ are introduced to ensure that all state variables, i.e. the variables without asterisks, are benchmarked to the same base period. In our application below, we will choose this to be the pre-industrial period, represented by the year 1750. This means that μ_m , for instance, denotes the offset needed in the observations $T_t^{m,*}$ to benchmark these to the pre-industrial period, i.e. $T_t^{m,*} - \mu_m$ is the surface temperature anomaly relative to this period. The last measurement equation for ocean heat content O_t^* is obtained from the relationship

$$H_d \frac{dT_t^d}{dt} = \frac{dO_t}{dt},$$

(e.g. Schwartz, 2007; Bennedson et al., 2023) and the fact that the observation time series $T_t^{d,*}$ and O_t^* are anomalies assumed to be benchmarked to the same historical period.

3.3 State space representation

Let $y_t = (C_t^*, S_t^{OCN,*}, S_t^{LND,*}, F_t^{CO2,*}, T_t^{m,*}, T_t^{d,*}, O_t^*)'$ denote the 7×1 vector of observations at time t . The resulting non-linear state space model for the climate system described in Section 2 is

$$y_t = \mu + Ax_t + \epsilon_t, \quad x_{t+\Delta} = B(x_t) + W_t + R\eta_{t,\Delta},$$

where the 7×1 vector μ contains the intercepts in the measurement equations of Section 3.2, the 7×6 matrix A enables the appropriate selection of the element in the 6×1 state vector $x_t = (C_t, S_t^{OCN}, S_t^{LND}, F_t^{CO2}, T_t^m, T_t^d)'$ for each variable in y_t , the 7×1 vector ϵ_t contains the measurement errors listed in Section 3.2, the 6×1 non-linear vector function $B(\cdot)$ captures the non-linear dynamic equations for the latent state variables in Section 3.1, the 6×1 vector W_t consists of zeros and composite covariates such as $\Delta(F_t^{CO2} + F_t^{Ex})/H_m$, and the 6×5 matrix R selects the appropriate element from the 5×1 innovation vector $\eta_{t,\Delta} = (\eta_t^O, \eta_t^L, \eta_t^F, \eta_t^m, \eta_t^d)'$.

The state update equation comprises the dynamic processes of the physical quantities in Section 3.1. The measurement error sequence ϵ_t captures the transitory deviations between observations and the corresponding underlying state processes. We allow each element in ϵ_t to be a serially correlated sequence modelled as a first-order stationary autoregressive process, that is

$$\epsilon_{t+\Delta} = \Phi\epsilon_t + \xi_{t,\Delta}, \quad \xi_{t,\Delta} \stackrel{iid}{\sim} N(0, \Delta \cdot P),$$

where the autoregressive coefficient matrix Φ is diagonal, $N(0, V)$ refers to the multivariate normal distribution with a zero mean vector and variance matrix V , and *iid* means *independent and identically distributed*. To impose the stationarity of ϵ_t , we assume that each diagonal element of Φ is smaller than unity in absolute value. Given that variance matrix $P = Var(\xi_{t,\Delta})/\Delta$, stationarity implies that $Var(\epsilon_t) = (I - \Phi^2)^{-1}P$. A detailed discussion on the dynamic specification of ϵ_t is presented in Section 5.1. We further have the innovation sequence

$$\eta_{t,\Delta} \stackrel{iid}{\sim} N(0, \Delta \cdot Q),$$

with diagonal variance matrix Q , in recognition that the physical equations in Section 3.1 are only approximations to the true climate system. It follows that $R\eta_{t,\Delta} = x_{t+\Delta} - B(x_t) - W_t$ can be regarded as the error between the “true” climate system and our simplified non-linear version of it. More details on the entities $\{A, B(\cdot), R, \Phi, P, Q\}$, and how they are specified in the Stat-RCM, are provided in Appendix A. The fixed unknown constants and coefficients are collected in the parameter vector θ and are estimated by the method of maximum likelihood, where the extended Kalman filter is used to evaluate the likelihood function. We refer to Durbin and Koopman (2012, Chapter 10) for further details on this approach to estimation.

4 Monte Carlo simulation study

We perform a Monte Carlo simulation study designed to gauge the finite sample performance of the maximum likelihood estimation method in a controlled setting. We use the historical CO₂ emissions and forcing data over the period 1959–2022 as the covariates in the Stat-RCM model; see Section 5 for a more in-depth discussion on these data. We then simulate the stochastic processes ϵ_t and η_t from their specifications provided in Section 3.3, and use these to generate simulated paths for the state vector x_t and the observation vector y_t over the period 1959–2022, resulting in $n = 64$ observations. The model parameters used for simulation are set equal to the estimates we have

Table 1: *Monte Carlo simulation results*

	b_1	b_2	c_1	c_2	f_1	γ	λ	H_m	H_d	μ_m	μ_d
True values:	0.01	0.02	0.09	0.09	5.58	1.44	1.44	8.97	265.88	0.28	0.05
MC Avg	0.01	0.02	0.08	0.10	5.58	1.24	2.21	8.23	265.81	0.39	0.11
(MC Std.)	(0.00)	(0.00)	(0.03)	(0.05)	(0.01)	(0.64)	(1.25)	(2.81)	(0.25)	(0.17)	(15.78)

Simulation results for physical parameters $\tilde{\theta} = (b_1, b_2, c_1, c_2, f_1, \gamma, \lambda, H_m, H_d)'$ as well as the constant offsets μ_m and μ_d . Number of Monte Carlo replications is 1000 and number of observations is $n = 64$. The first row reports the true parameters used for simulating the paths of the state and measurement variables and the second and third row report the Monte Carlo average and Monte Carlo standard deviation, respectively, calculated over the 1000 replications.

obtained from our empirical study in Section 5. In particular, we have set $\mu_C = \mu_L = \mu_O = \mu_F = 0$ and $f_2 = f_3 = 0$. The remaining parameters are estimated freely by numerically maximizing the likelihood function obtained by the extended Kalman filter. We repeat this simulation-estimation process 1000 times to obtain 1000 Monte Carlo estimates of the parameters of the model.

Table 1 summarizes the results of the simulation experiment, where we focus on the estimates of the physical parameters in the model, $\tilde{\theta} = (b_1, b_2, c_1, c_2, f_1, \gamma, \lambda, H_m, H_d)'$, and the constant offsets μ_m and μ_d . Figure 2 presents histograms of the 1000 estimates for each of the parameters in $\tilde{\theta}$, where a vertical red line indicates the ‘true’ data-generating value of the respective parameter. We can conclude that the parameters of the carbon cycle module $\{b_1, b_2, c_1, c_2\}$ and forcing equation $\{f_1\}$ are estimated with a high degree of precision. The parameters from the energy balance module $\{\gamma, \lambda, H_m, H_d\}$, as well as the constant offsets $\{\mu_m, \mu_d\}$, appear more difficult to estimate. In particular, the estimates of H_m and H_d appear to show some small-sample bias. Overall, the finite sample properties of the estimation procedure are adequate in this Monte Carlo study design and this choice of parameter values.

5 The performance of Stat-RCM on the 1959-2022 historical record

We consider a historical yearly time series data set from 1959 to 2022. The data for the carbon cycle $\{C_t^*, S_t^{OCN,*}, S_t^{LND,*}, E_t^{FF}, E_t^{LUC}\}$ are from the Global Carbon Project (Friedlingstein et al., 2022)². The forcing data $\{F_t^{CO2,*}, F_t^{Non-CO2}, F_t^{Nat}\}$ are the current best estimates taken from the Sixth Assessment Report (AR6) of the IPCC (Smith et al., 2021)³. The global mean surface

²<https://www.globalcarbonproject.org>.

³https://zenodo.org/record/5705391#.ZF1x_y9ByX2.

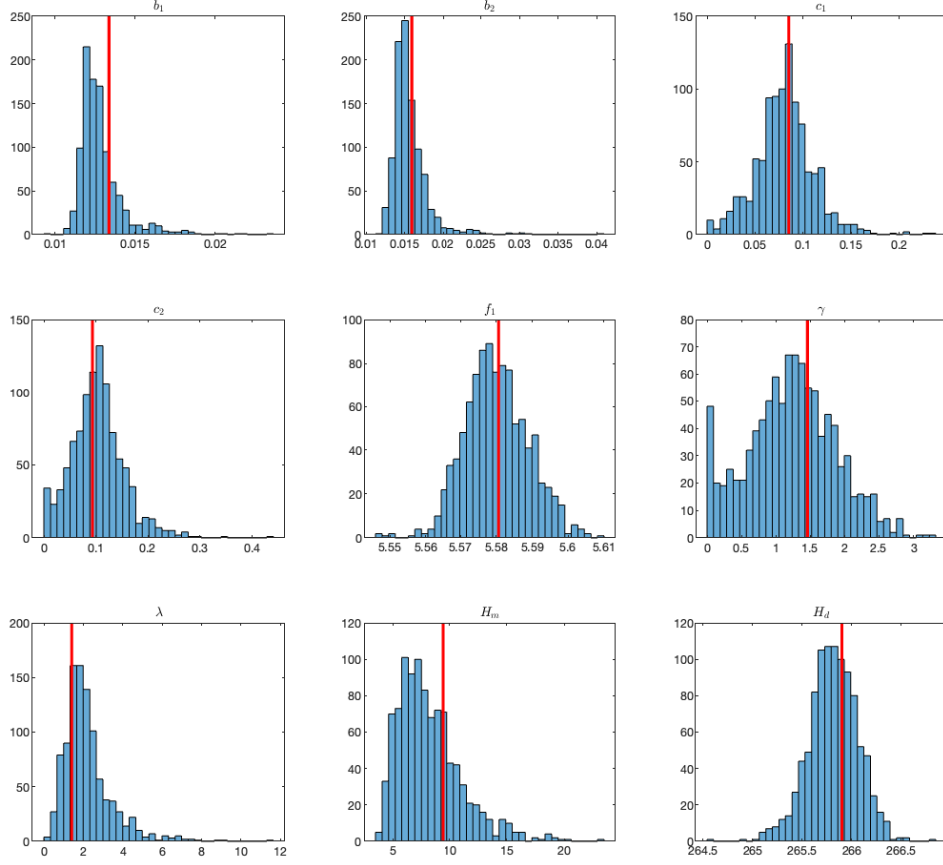


Figure 2: Histogram of the parameter estimates of $\tilde{\theta} = (b_1, b_2, c_1, c_2, f_1, \gamma, \lambda, H_m, H_d)'$ obtained from 1000 Monte Carlo replications, see Section 4. The vertical red line indicates the true parameter used as data generating value in the simulations.

temperature data ($T_t^{m,*}$) are from HadCRUT5 by the Met Office Hadley Centre (Morice et al., 2020)⁴. The deep ocean temperature data ($T_t^{d,*}$) and the ocean heat content data (O_t^*) are from the Institute of Atmospheric Physics (IAP; Cheng et al., 2017)⁵.

The AR6 forcing data of Smith et al. (2021) end in 2019 while our remaining data run until 2022. For the forcing variable F_t^{CO2} , which is a model variable, it does not pose an issue since the Kalman filter and smoother can easily handle missing data values. For the covariates, including the forcing variables $F_t^{Non-CO2}$ and F_t^{Nat} , however, we need a complete data record. We therefore

⁴<https://www.metoffice.gov.uk/hadobs/hadcrut5/data/HadCRUT.5.0.2.0/download.html>.

⁵<http://www.ocean.iap.ac.cn/>, all data resources 1-4 are last accessed on March 13, 2024.

impute the 2020–2022 values of $F_t^{Non-CO_2}$ and F_t^{Nat} using a linear trend, estimated from the last five years of the data, i.e. 2015–2019. The results obtained from the Stat-RCM, reported below, are robust to alternative approaches to filling in these missing values. This is not surprising since the forcing from CO₂ is much larger in magnitude than the forcing from non-CO₂ greenhouse gases and natural forcing.

The carbon cycle data from the Global Carbon Project and the forcing data for the AR6 report are benchmarked to 1750, meaning that we may set $\mu_C = \mu_L = \mu_O = \mu_F = 0$. We benchmark the surface temperature data, $T_t^{m,*}$, to the base period 1850–1900 and the deep ocean data, $T_t^{d,*}$ and O_t^* , to 1940. To ensure that the state variables T_t^m and T_t^d are benchmarked to 1750, we include the offset parameters μ_m and μ_d in the relevant measurement equations and estimate these freely.

5.1 The dynamic specification of the error structure

In Section 3.3, we have modelled the stochastic error variables in the 7×1 vector ϵ_t as autoregressive processes of order 1. This type of process falls into the class of the autoregressive moving average (ARMA) processes which is well-known in time series analysis (Brockwell and Davis, 1996). The ARMA model can have different maximum lag lengths for the autoregressive part, denoted by p , and for the moving average part, denoted by q . We first have considered the ARMA specification, with $p = q = 1$, for each error term in ϵ_t . In addition, we have included a correlation coefficient, ρ , between the ARMA innovation term ξ_t (see also Section 3.3) associated with the measurement equations for T_t^d and O_t . These two variables are closely related and therefore this dependence is introduced, see also Bennedsen et al. (2023). The initial estimates of the ARMA parameters have revealed that parameters of the moving average part are statistically insignificant at the 10% level, while those of the autoregressive part are significant. We therefore have opted for the autoregressive part only and obtained the specification for ξ_t as in Section 3.3, also see Appendix A for further details. The estimate of the dependence coefficient ρ is statistically significant and therefore it is kept in the specification for ξ_t .

5.2 Model selection: the forcing equation

The Beer-Lambert law suggests that the functional relationship between atmospheric CO₂ concentration and radiative forcing from CO₂ is approximately logarithmic (Lightfoot and Mamer, 2014). Various functional forms have been suggested to improve upon this approximation (e.g. Hansen et al., 1988; Shi, 1992; Hansen et al., 1998). As discussed in Section 2.2, there appears to

be no consensus in the RCM literature on which of these functional forms is most adequate for describing the link between atmospheric concentrations and radiative forcings. Here, we will adopt statistical model selection methods to determine which functional form is most appropriate for the historical data under study. To the best of our knowledge, statistical model selection methods have not been used to inform the construction of RCMs previously. Given the statistical formulation of the Stat-RCM, model selection is relatively straightforward to carry out.

In relation to the forcing equation (2.3), that is $g_F(C_t) = f_1 \log(C_t + f_2 C_t^2) + f_3 \sqrt{C_t}$, we are interested in testing the hypotheses

$$H_0^{sqr} : f_1 = f_2 = 0,$$

$$H_0^{log} : f_2 = f_3 = 0,$$

$$H_0^{log+sqr} : f_2 = 0,$$

$$H_0^{log^2} : f_3 = 0,$$

$$H_0^{Hansen98} : f_1 = 5.04, f_2 = 0.00023507, f_3 = 0.$$

The two hypotheses H_0^{sqr} and H_0^{log} can be used to test whether the forcing equation reduces to a square root function and a logarithmic function, respectively. The hypothesis H_0^{log} reduces the forcing equation to the one used in MAGICC6 (Meinshausen et al., 2011, p. 1439). Under the hypothesis $H_0^{log+sqr}$, the forcing equation is the sum of a square root term and a logarithmic term, which is the forcing equation used in the FaIR RCM (Leach et al., 2021, p. 3013). The forcing equation implied by $H_0^{log^2}$ is proposed in Hansen et al. (1998). The hypothesis $H_0^{Hansen98}$ implies the same forcing equation, but where the parameters are fixed to the specific values used in Hansen et al. (1998).⁶ See also Ramaswami (2001, Table 6.2., p. 358) for various suggestions for expressions of the forcing equation, including some of those studied here.

Since the models implied by the hypotheses listed above are nested in the general forcing equation (2.3), where f_1 , f_2 and f_3 are unrestricted coefficients, we can perform the various hypothesis tests using a standard likelihood ratio test. Table 2 contains the maximized log-likelihood values for the models with different forcing specifications, together with the Bayesian Information Criteria

⁶Table 1 of Hansen et al. (1998) actually specifies the forcings function $g_F(c_t) = 5.04 \log(c_t + 0.0005c_t^2)$, where c_t is atmospheric concentrations given in ppm. Since $C_t = c_t \cdot 2.127\text{GtC/ppm}$, this translates into the parameters $f_1 = 5.04$ and $f_2 = 0.0005/2.127 = 0.00023507$ in our framework. When estimating the parameters from this forcing equation, i.e. when working under $H_0^{log^2}$, we find $\hat{f}_1 = 5.58$ and $\hat{f}_2 = 0.00000105$, indicating that the forcing data used in this paper results in somewhat different parameter estimates than what was used in Hansen et al. (1998).

Table 2: Likelihood ratio tests for the forcing equation

	Unrestricted	$H_0^{sqr+log}$	H_0^{log2}	H_0^{sqr}	H_0^{log}	$H_0^{Hansen98}$
Maximized log-likelihood:	925.79	924.78	923.77	917.17	923.76	911.21
Bayesian Information Criterion:	-1714.34	-1716.48	-1714.45	-1705.41	-1718.60	-1697.67
Number of parameters:	33	32	32	31	31	30
p -value (Likelihood Ratio test):	-	0.1552	0.0444	0.00018	0.1313	0

The Likelihood Ratio tests are against the “unrestricted” model with coefficients f_1 , f_2 and f_3 estimated freely.

(BIC; Schwarz, 1978), the numbers of estimated parameters, and the p -values for the likelihood ratio tests. We find that the model specification under H_0^{log} : $f_2 = f_3 = 0$ above has the lowest BIC value and hence has most support from the data. The two hypotheses H_0^{sqr} and $H_0^{Hansen98}$ can formally be rejected at a 1% significance level and H_0^{log2} barely at a 5% level. The rejection of H_0^{sqr} indicates that a log-term is preferred to a square root term when modelling the relationship between atmospheric CO₂ concentrations and radiative forcing, for this updated AR6 forcing data set. Finally, the rejection of $H_0^{Hansen98}$ indicates that the parameter values used in Hansen et al. (1998) do not fit this data set.

The reported results below are based on the model specification under H_0^{log} as it produces the lowest BIC value, and is not rejected by the likelihood ratio test. The model specifications with a comparable fit as the H_0^{log} model, that is the model implied by $H_0^{log+sqr}$ and H_0^{log2} and the unrestricted model, yield similar results as those from the model with H_0^{log} .

5.3 Estimation results and assessment of model fit

Given the findings from the model selection exercise above, we work under the hypothesis H_0^{log} , i.e. we set $f_2 = f_3 = 0$ and estimate the parameter f_1 in the forcing equations (2.2)–(2.3) together with the other parameters. The estimation results from this model applied to the 1959–2022 data are presented in Table 3. For purposes of brevity, we only present the estimates from the “physical” parameters in the model, i.e. the parameters governing the main workings of the carbon cycle module, $\{b_1, b_2, c_1, c_2\}$, the forcing module, f_1 , the energy balance module, $\{\gamma, \lambda, H_m, H_d\}$, as well as the constant offsets from the measurement equations $\{\mu_m, \mu_d\}$. Estimates of the remaining parameters are presented in Appendix B.

The signs and magnitudes of the estimated carbon cycle feedback parameters $\{b_1, b_2\}$ are as anticipated and are found in previous studies (e.g. Bennedsen et al., 2023). The climate feedback parameters $\{c_1, c_2\}$ are both estimated as $\hat{c}_1, \hat{c}_2 \approx 0.09$, implying that a temperature rise of 1°C,

above pre-industrial levels, would correspond to a climate feedback factor of $\exp(-T_t^m \cdot \hat{c}_i) = \exp(-1 \cdot 0.09) \approx 0.9139$, for $i = 1, 2$. This is roughly a 9% weakening of the sinks compared to pre-industrial levels (notice that $T_{1750}^m = 0$). A similar magnitude of the climate feedback estimate obtained from historical data has been reported previously (Zhang et al., 2021) but it is lower than values found using large-scale climate models (Friedlingstein, 2015). The reason for the low estimate of the climate feedback effect in the Stat-RCM is probably due to the input data used, i.e. the historical data 1959–2022, where climate feedback effects are still rather weak. To obtain more precise estimates of the climate feedback effect would require data where these feedbacks are more manifest. This could for instance be achieved by fitting the Stat-RCM to output from large-scale climate models run over longer periods than the historical period, similar to what is done for other RCM emulators (Nicholls et al., 2020). This avenue is left for future research.

In Table 3, we present the results for the forcing module and we find that the estimated parameter \hat{f}_1 is highly significant and has the expected sign. The parameter estimates from the energy balance module align well with previous studies (Cummins et al., 2020; Pretis, 2020; Bennedsen et al., 2023). We notice that an estimate of the equilibrium climate sensitivity (ECS) can be derived from our estimate of the climate feedback parameter λ . In particular, the IPCC Sixth Assessment Report (AR6; Forster et al., 2021) suggests the relationship $ECS = F_{2 \times CO_2} / \lambda$, where $F_{2 \times CO_2}$ is the radiative forcing in response to a doubling of CO_2 concentrations in the atmosphere. Using the best estimate of $\hat{F}_{2 \times CO_2} \approx 3.93$ (± 0.47 , 5%–95% CI) Wm^{-2} from AR6 (updated), we find that $\widehat{ECS} = F_{2 \times CO_2} / \hat{\lambda} = 3.93 / 1.42 = 2.78^\circ C$. This estimate aligns well with the “likely” range of 2.5° – $4.0^\circ C$ obtained from instrumental records and reported in AR6 (Forster et al., 2021). Under certain assumptions, we can also obtain the (asymptotic) variance of \widehat{ECS} which results in a standard error of 1.03.⁷ Hence, the Stat-RCM estimate and associated standard error of equilibrium climate sensitivity is $\widehat{ECS} = 2.78$ with standard error of 1.03.

For a correctly specified model, the standardized one-step ahead prediction residuals will be a sequence of iid $N(0, 1)$ variables (Durbin and Koopman, 2012). Diagnostics on these standardized prediction residuals are presented in Table 4. There appears to be some autocorrelation left in the

⁷The standard error of \widehat{ECS} can be obtained as follows. Define $\widehat{ECS} = g(\hat{F}_{2 \times CO_2}, \hat{\lambda}) = \hat{F}_{2 \times CO_2} / \hat{\lambda}$, where $g(x, y)$ is the function $g(x, y) = x/y$. The Jacobian of g is $\partial g = (1/\hat{\lambda}, -\hat{F}_{2 \times CO_2} / \hat{\lambda}^2)'$. Let Σ be the 2×2 diagonal matrix with $Var(\hat{F}_{2 \times CO_2})$ and $Var(\hat{\lambda})$ on the diagonal. An estimate of $Var(\hat{\lambda})$ can be obtained from the maximum likelihood method discussed in Section 3.3. Assuming Gaussian distributions and a 90% confidence interval of (3.93 ± 0.47) as reported in Forster et al. (2021), we obtain the estimate $\widehat{Var}(\hat{F}_{2 \times CO_2}) = (0.47/1.6449)^2$. The variance of \widehat{ECS} can then be approximated via the ‘delta method’ as $\widehat{Var}(\widehat{ECS}) = (\partial g)' \Sigma \partial g$.

Table 3: *Stat-RCM parameter estimates*

	b_1	b_2	δ_1	δ_2	f_1	γ	λ	C_m	C_d	μ_m	μ_d
Estimate:	0.01	0.02	0.08	0.09	5.58	1.46	1.42	9.37	265.90	0.30	0.20
Std. Err.:	(0.00)	(0.00)	(0.02)	(0.04)	(0.01)	(0.58)	(0.51)	(2.44)	(0.41)	(0.41)	(0.36)
t -stat:	11.25	7.83	5.16	2.53	580.42	2.51	2.75	3.84	656.40	0.74	0.55

Parameter estimates by the maximum likelihood method applied to the 1959–2022 data.

Table 4: *Residual diagnostics*

y	Mean	Std.	Skew	Kurt	SC	JB	DW	LB(1)	LB(5)	LB(10)	ARCH
C	−0.01	1.08	−0.28	3.02	0.03	0.81	1.93	0.08	1.72	12.17	0.01
OCN	−0.06	1.00	−0.18	2.35	0.14	1.45	1.71	1.07	6.64	8.51	0.18
LND	−0.07	0.92	0.17	2.65	−0.09	0.62	2.18	0.64	17.10	47.91	1.63
Forc	0.02	1.01	−0.55	3.94	0.05	5.20	1.89	0.13	2.06	6.51	5.29
Temp	−0.01	1.00	0.06	2.40	−0.01	0.98	2.01	0.01	7.19	15.48	0.01
O-Temp	0.04	0.99	−0.25	2.62	−0.18	1.05	2.37	2.27	10.30	17.38	2.88
OHC	0.04	1.00	−0.25	2.63	−0.18	1.03	2.37	2.29	10.39	17.36	2.86

Diagnostics of standardized one-step ahead prediction residuals as output from the extended Kalman filter. SC is the estimate of the serial correlation coefficient ϕ in the regression $y_t = \phi y_{t-1} + \epsilon$; JB is the Jarque-Bera test statistic (Jarque and Bera, 1987): the null hypothesis of Gaussianity is rejected if JB is larger than the 95% critical value of 5.99. DW is the Durbin-Watson test statistic (Durbin and Watson, 1971): $DW < 2$ indicates positive serial correlation, $DW > 2$ negative serial correlation; $DW = 2$ indicates no serial correlation. $LB(p)$ is the Ljung-Box Q test statistic (Ljung and Box, 1978) for autocorrelation, calculated using p lags. The 95% critical value of the LB test are 3.84, 11.07, 18.31 for $p = 1, 5, 10$, respectively. $ARCH$ is the test statistic of the Engle (1988) test for heteroskedasticity. The 95% critical value of the $ARCH$ test is 3.8415.

prediction residuals at the longer lags for the land sink. The predictions residuals from the forcing equation display some indications of non-Gaussianity and heteroskedasticity due to outliers in the early 1970s. Overall, however, the diagnostics are very reasonable and indicate that the model is able to fit the data well. The raw data, along with smoothed states as output from the extended Kalman filter, are presented in Figure 3. The standardized one-step ahead prediction residuals used for the residual diagnostics in Table 4 are displayed in Figure 4.

5.4 State estimation

The Kalman filter methodology allows for the efficient estimation of the latent variables in the 7×1 state vector x_t . In particular, the state estimate obtained from the Kalman smoother is an estimate of $E[x_t|y_{1959:2022}]$ for $t = 1959, 1960, \dots, 2022$, where x_t denotes the state at time t and

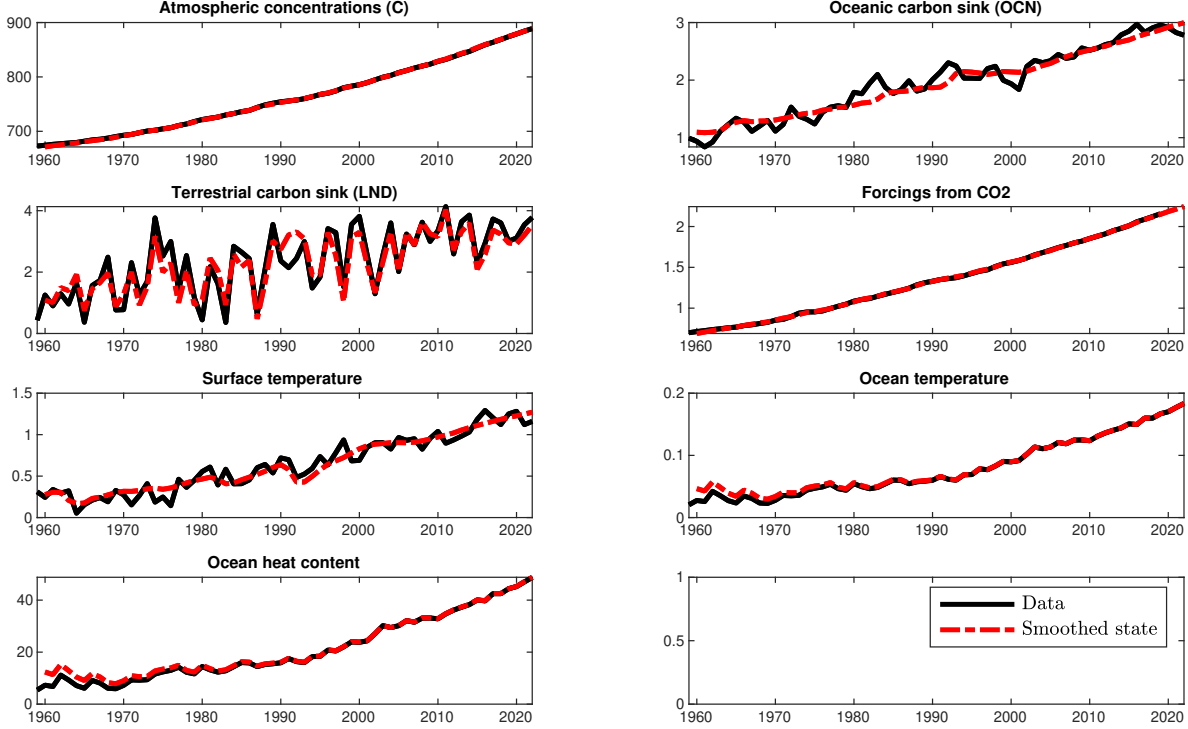


Figure 3: Smoothed states from the Stat-RCM (red dashed lines), estimated on the historical data record 1959–2022 (black lines), as output from the extended Kalman smoother. For surface temperature, ocean temperature, and ocean heat content, the estimated constant offsets ($\mu_m, \mu_d, H_d \cdot \mu_d$) have been added to the smoothed states to make them comparable to the data.

$y_{1959:2022}$ denotes the full historical data set. These smoothed states are presented in Figure 3.

The estimated state for the surface temperature T_t^m , i.e. $\hat{T}_t^m = \hat{E}[T_t^m | y_{1959:2022}]$ for $t = 1959, 1960, \dots, 2022$, can be seen as an estimate of the underlying long-term temperature anomaly, i.e. an estimate where transitory effects, such as measurement errors, captured in our model by the error process ϵ_t , have been filtered out. Thus, our estimate of the surface temperature state can serve as a broad indicator of the overall state of the climate. In this way, it can be used to assess how close we are to breaching international temperature agreements such as the 2015 Paris Agreement of keeping “global temperatures well below 2°C above pre-industrial times while pursuing means to limit the increase to 1.5°C” (UNFCCC, 2015). Assessment and detection of whether temperature targets have been breached is difficult, due to the inherent noisiness and variability of temperature measurements (Betts et al., 2023). In AR6, the IPCC itself proposed a way of detection such as breach: *A breach is deemed detected if the average temperature over a 20-year horizon exceeds the target* (e.g. IPCC, 2023). This means that there will be a long lag, on the order of a decade, before a

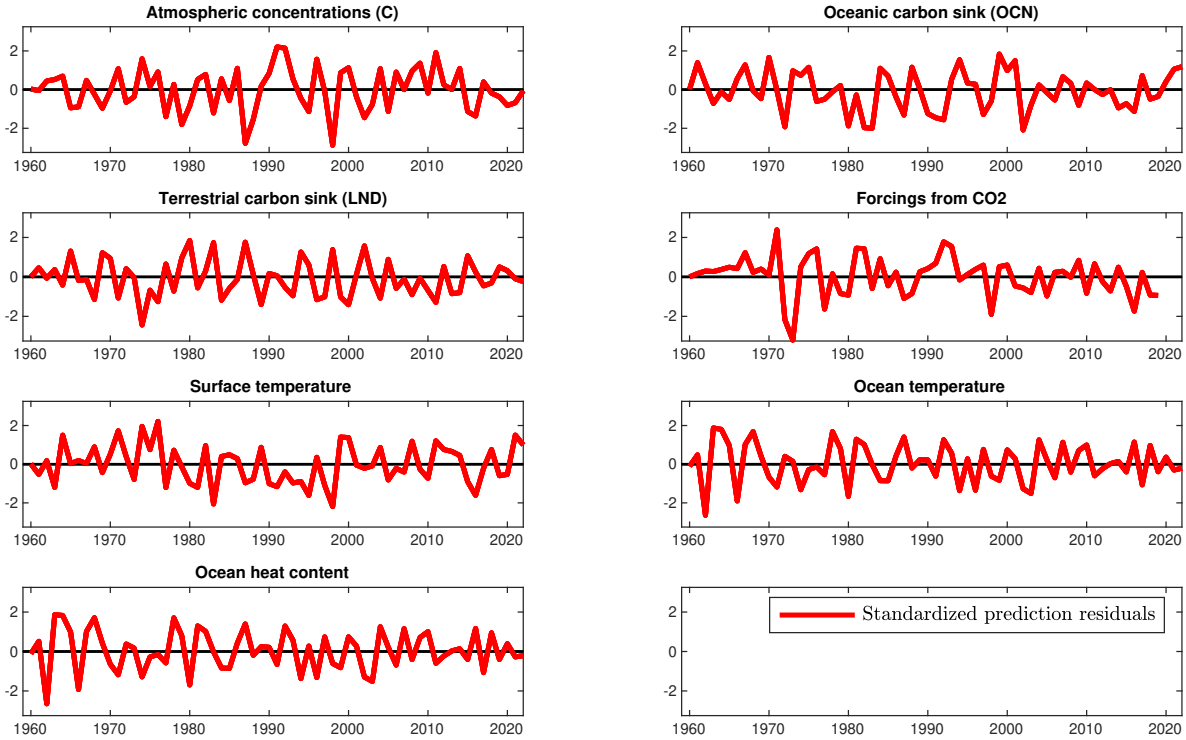


Figure 4: *Standardized one-step ahead prediction residuals from the Stat-RCM estimated on the historical data record 1959–2022.*

breach of a temperature target will be detected. Such slow detection times run the risk of delaying action that may be relevant in case of a breach. For this reason, several methods have recently been suggested, which are able to monitor the underlying global temperature level closer and offer faster detection times of possible breaches. For instance, [Betts et al. \(2023\)](#) suggests to blend the past 10 years of historical temperature data with projections of the next 10 years of temperature data, obtained from a climate model. While this method is able to estimate a “20-year average” of the current temperature level without delay, it has the downside that the credibility of the estimate depends on the projected temperature, which in turn depends on the climate model used to construct the projections. Alternative methods for keeping track of current underlying global temperatures include Copernicus’ approach of calculating a 30-year linear trend into the future,⁸ NASA’s approach of using lowess smoothing,⁹ and the “Real-time Global Warming Index” of [Haustein et al. \(2017\)](#), which estimates the amount of warming due to anthropogenic causes by regressing temperature data on forcing time series.

⁸<https://cds.climate.copernicus.eu/apps/c3s/app-c3s-global-temperature-trend-monitor?month:float=10&year:float=2>

⁹<https://climate.nasa.gov/vital-signs/global-temperature/>

In contrast, the estimated temperature state from the Stat-RCM can be seen as a purely statistical and data-driven alternative to assess the current level of underlying warming above pre-industrial levels. This estimate is only based on historical data and it is compatible with the physical components of the Stat-RCM, i.e. the carbon cycle module, the forcing module, and the energy balance module. Based on the data used in this paper, the current best-estimate of the underlying warming above the 1850–1900 baseline (the baseline usually used for defining temperature targets), obtained from the Stat-RCM, is $\hat{T}_{2022}^m + \hat{\mu}_m = \hat{E}[T_{2022}^m | y_{1959:2022}] + \hat{\mu}_m = 1.27^\circ\text{C}$. This number is substantially above the 2022 temperature measurement, $T_{2022}^{m,*} = 1.16$, see Figure 3. This is mostly due to the 2022 La Niña conditions which have been filtered out of the estimate $\hat{T}_{2022}^m = \hat{E}[T_{2022}^m | y_{1959:2022}]$, leading to a more precise representation of the underlying warming trend, i.e. a trend free from transitory deviations such as ENSO.

6 Scenario projections using Stat-RCM

We compute scenario projections of the future climate system from the estimated Stat-RCM, conditional on paths for the covariate (external) variables CO₂ emissions, forcing from non-CO₂ greenhouse gases, and forcing from natural sources. We focus particularly on the probabilistic projections. Section 6.1 lays out the projection methodology, which is based on simulations from the estimated Stat-RCM. Section 6.2 contains a validation exercise, where we use historical covariates from the period 1959–2022 and investigate whether the Stat-RCM is able to produce “projections” over 1959–2022 that agree with the historical data record. Section 6.3 presents scenario projections for 2023–2100 in a setting where CO₂ emissions are rapidly declining, a necessary condition for halting global warming and achieving the goals as set out by international agreements, such as the Paris Agreement (e.g. Sanderson et al., 2016; Luderer et al., 2018; Tokarska and Gillett, 2018).

6.1 Epistemic and aleatoric uncertainty in climate projections

To gauge the degree of uncertainty introduced by the separate stochastic parts of the Stat-RCM, we consider the following four different approaches of using the model to project the climate system forward, conditional on paths of all covariate variables.

1. Deterministic run: Deterministic projection where the parameters of the Stat-RCM, θ , are set to their maximum likelihood estimates as reported in Section 5, and based on the 1959–2022 data; we have $\theta = \hat{\theta}$ and all error processes are set to zero, $\epsilon_t = \eta_t = 0$ for all t .

2. Uncertainty coming from unknown parameters (θ): Projection where the physical parameters, $\tilde{\theta} = (b_1, b_2, c_1, c_2, f_1, \gamma, \lambda, H_m, H_d)'$, are randomly sampled from the asymptotic distribution, that is $\tilde{\theta} \sim N(\hat{\theta}, \hat{\Sigma})$, where $\hat{\theta}$ and $\hat{\Sigma}$ are the maximum likelihood estimates of the physical parameters and their variance-covariance matrix, based on the 1959–2022 data. The remaining parameters are set equal to their maximum likelihood estimates. The error processes are set to zero, i.e. $\epsilon_t = \eta_t = 0$ for all t .
3. Uncertainty coming from unknown parameters and state innovations (θ, η): Similar to the setup in 2, but now adding the stochastic variation due to the innovation terms in the state equations η , and setting the measurement error processes to zero i.e. $\epsilon_t = 0$ for all t .
4. Uncertainty coming from unknown parameters, state innovations, and measurement errors (θ, η, ϵ): Similar to the setup in 3, but now adding the stochastic variation due to the measurement errors ϵ_t .

In the first setup, the projection is deterministic, conditional on estimated parameters and input paths of the covariates. The next three setups contain stochastic variation to increasing degrees: First, by considering only randomness arising from the uncertainty in parameters (θ), then also including uncertainty coming from the evolution of the state equations (θ and η), and finally also including the uncertainty coming from other processes, such as measurement errors and ENSO effects (θ, η and ϵ). We refer to the uncertainty about parameters as “epistemic” uncertainty, in the sense that this uncertainty reflects our ignorance of the data generating process behind the climate system, while uncertainty stemming from the error processes η and ϵ may be referred to as “aleatoric”, in the sense that this uncertainty captures the internal random variability of the climate system itself. To construct projections and confidence bands from the model under the various uncertainty specifications, we simulate 10^5 different instances of the variables in the model using given paths for the covariates and plot the pointwise quantiles of 2.5%, 50% and 97.5%.

6.2 Validation exercise

We adopt the model specification and its parameter estimates as reported in Section 5 for the period 1959–2022, to perform a validation exercise. We take the covariates CO2 emissions (E_t), forcing from non-CO2 sources ($F_t^{Non-CO2}$), and forcing from natural sources (F_t^{Nat}) as inputs and keep them fixed to their historical values. The projection results are presented in Figure 5. The top left panel shows the covariates (input variables) and the remaining panels show the quantiles of

the simulated model variables, along with the original observations (red) used for the estimation of the model superimposed. Although the original observations are used for the parameter estimates, we stress that they are not otherwise used as input for this validation exercise. From Figure 5, we find that the model is well-validated over the estimation sample 1959–2022, in the sense that it can produce simulations of the climate system with a high degree of similarity to the observed historical data.

6.3 Projections to 2100 in a strong mitigation scenario

Next, we use the Stat-RCM to project the variables until the year 2100, conditional on given future paths for the covariates of CO₂ emissions, forcing from non-CO₂ greenhouse gases, and natural forcing. The path for CO₂ emissions is taken from the SSP119 scenario (Meinshausen et al., 2020), and forcings from non-CO₂ greenhouse gases consistent with SSP119 are obtained from the MAGICC RCM.¹⁰ The path for future natural forcing is set constant equal to the last in-sample value. The values for the future paths of the covariates are shown in the top-left panel of Figure 6, where a solid line denotes historical data, from which the parameter estimates for Stat-RCM are obtained, and dashed lines denote the future scenario used in the projection of the model. We notice that the SSP119 scenario is very ambitious in the sense that it implies rapid reductions in greenhouse gas emissions in the short term, and substantial carbon dioxide removal from the atmosphere (negative emissions) in the long term.

We assess the uncertainty using 10^5 simulated trajectories of the model, see also Section 6.1. Figure 6 shows the projection results for all the climate state variables output by Stat-RCM. To visualize how the the different layers of uncertainty impact the projections, Figure 7 contains the first 50 simulated trajectories in the case of surface temperature, T^m . The left panel of Figure 7 includes only uncertainty coming from parameters (θ), while the middle panel additionally includes uncertainty coming from the innovations in the state equation (θ, η), and the right panel adds uncertainty from the measurement errors (θ, η, ϵ). From the left panel, we learn that uncertainty coming from parameters (θ) is substantial. The resulting simulated trajectories are very smooth, due to the absence of stochastic innovations in these simulations. From the middle panel, we learn that adding uncertainty from the innovations in the state equation (θ, η) increases uncertainty

¹⁰The SSP119 scenario can be run in MAGICC in a web browser via the link <https://live.magicc.org/scenarios/bced417f-0f7f-4bb7-8359-792a0a8b0368/overview>. Here, the forcing from non-CO₂ greenhouse gases can also be downloaded. Last accessed May 12, 2023.

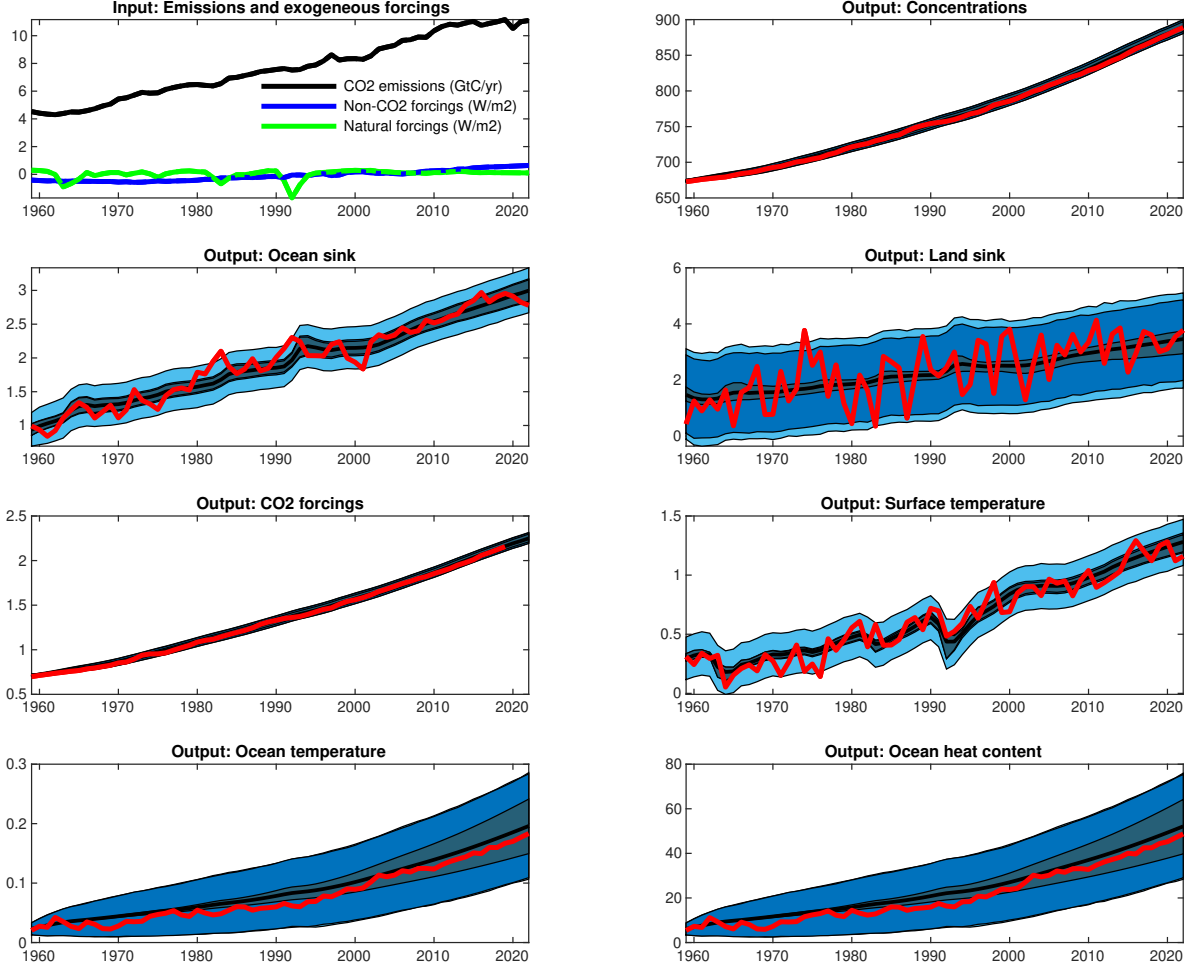


Figure 5: *Validation exercise using covariate data and estimated parameters from the historical data 1959–2022. Top left panel: Covariate input for the Stat-RCM. Remaining panels: Output of the Stat-RCM, including data (red lines) for comparison. Black line: Path of deterministic run (Setup in 1). Dark grey shading: 95% pointwise quantile bands for simulations with parameter uncertainty (θ ; Setup in 2). Dark blue shading: 95% pointwise quantile bands for simulations with uncertainty coming from parameters and innovations in the state equation (θ, η ; Setup in 3). Light blue shading: 95% pointwise quantile bands for simulations with uncertainty coming from parameters, innovations in the state equation, and transitory error terms (θ, η, ϵ ; Setup in 4).*

only slightly, which is to be expected since $\hat{\sigma}_{\eta, m}^2 = \text{Var}(\eta_t^m) \approx 0$ (see Table 5 in Appendix B). Conversely, from the right panel, we see that adding uncertainty from the measurement errors (θ, η, ϵ) increases uncertainty noticeably. These findings indicate that epistemic uncertainty is more important than aleatoric uncertainty for projections of the underlying surface temperature state

variable T_t^m , while aleatoric uncertainty is crucial in accounting for the variability in observations of surface temperatures, $T_t^{m,*}$.

We may use the model to assess the probability of particular events happening to the climate system in the future, such as surface temperatures exceeding predefined thresholds, given a scenario for the covariate processes. For instance, we might address the question “What is the probability of exceeding 1.5°C at some point in 2023–2100, given some future trajectory of CO₂ emissions and other covariate processes?” We can answer such questions using simulations similar to those above, by reporting the fraction of times the event in question happens in the simulations. Using this methodology for the SSP119 setting discussed in this section, the 1.5°C threshold is exceeded at some point in the period 2023–2100 with a 90% probability when considering uncertainty from all parts of the model (θ, η, ϵ) . When considering only uncertainty from parameters (θ) or uncertainty coming from parameters and innovations in the state equation (θ, η) , however, the probability drops to around 7% and 8%, respectively. The 50 simulated trajectories shown in Figure 7 illustrate how these numbers come about: When considering only uncertainty from parameters (θ) or from parameters and innovations in the state equation (θ, η) , the resulting trajectories are reasonably smooth (Figure 7, left and middle panels), while if uncertainty from measurement errors are included (θ, η, ϵ) , the resulting trajectories are very volatile (Figure 7, right panel). This volatility in the temperature measurements, arising e.g. from ENSO effects and other natural transitory processes, means that most trajectories will cross the 1.5°C threshold (denoted by the horizontal red line in Figure 7) at some point in the period 2023–2100. At the same time, the underlying long-term trend, absent the measurement error process ϵ , may plausibly stay below the threshold.

In summary, according to Stat-RCM, there is very high probability that the 1.5°C threshold will be breached by temperature observations $(T_t^{m,*})$ at some point over the period 2023–2100, but, if we filter out the transitory deviations from the underlying temperature trend, represented by ϵ , then there is, in fact, a very good chance that the underlying temperature trend (T_t^m) will stay below 1.5°C if the (very ambitious) SSP119 scenario is followed.

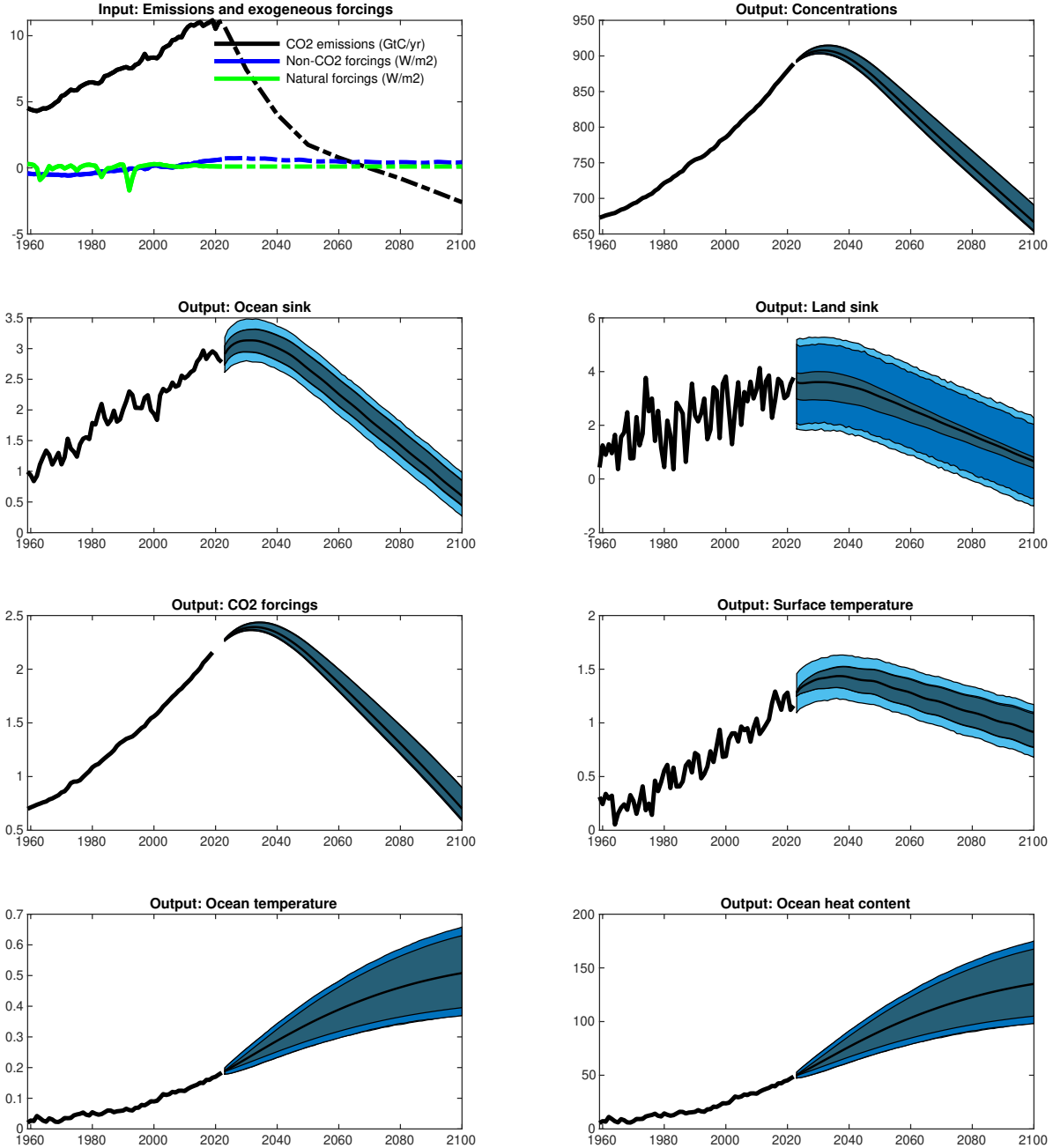


Figure 6: Projections as based on covariates emissions and forcing data from SSP119, 2023–2100, and Stat-RCM parameters estimated using historical data 1959–2022. Top left panel: Covariates input to the Stat-RCM. Remaining panels: Output of the Stat-RCM, including data for comparison. Black line: Path of deterministic run (Setup in 1). Dark grey shading: 95% pointwise quantile bands for simulations with parameter uncertainty (θ ; Setup in 2). Dark blue shading: 95% pointwise quantile bands for simulations with uncertainty coming from parameters and innovations in the state equation (θ, η ; Setup in 3). Light blue shading: 95% pointwise quantile bands for simulations with uncertainty coming from parameters, innovations in the state equation, and transitory error terms (θ, η, ϵ ; Setup in 4).

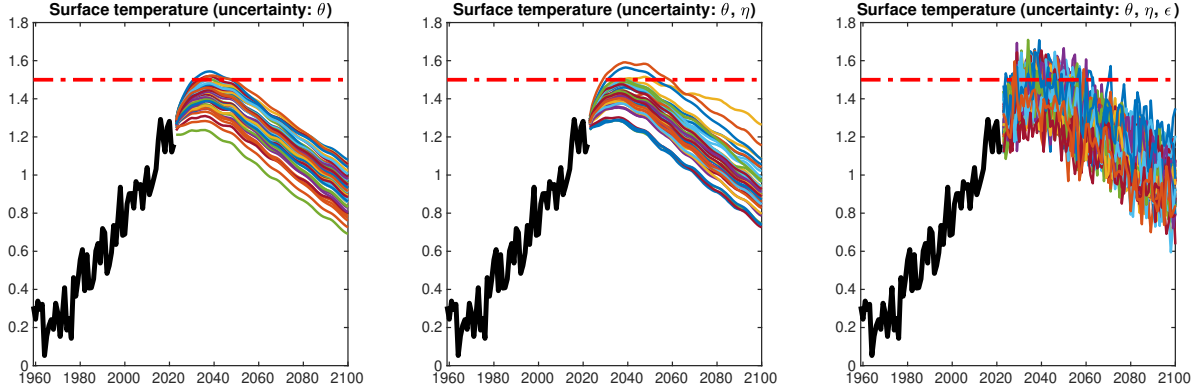


Figure 7: 50 simulated trajectories of the surface temperature anomaly T^m , benchmarked to the period 1850–1900. Black line: Historical data (1959–2022). Left panel: Simulations with parameter uncertainty (θ ; Setup in 2). Middle panel: Simulations with uncertainty coming from parameters and innovations in the state equation (θ, η ; Setup in 3). Right panel: Simulations with uncertainty coming from parameters, innovations in the state equation, and transitory error terms (θ, η, ϵ ; Setup in 4). Red dashed line denotes 1.5°C .

7 Conclusion

In this study, we have proposed a new statistical reduced-complexity climate model (Stat-RCM). We cast the Stat-RCM in a non-linear state space system that facilitates estimation, filtering, and smoothing using standard statistical methods (Durbin and Koopman, 2012). The model treats anthropogenic CO_2 emissions, forcing from other greenhouse gases, and natural forcing as covariates. The climate variables atmospheric concentrations, ocean sink, land sink, forcing from CO_2 , surface temperature, and deep ocean temperature are modelled as part of our climate model.

The stochastic formulation of Stat-RCM implies that tools from statistical theory are available. A Monte Carlo study has shown that the proposed estimation procedure, relying on maximizing the log-likelihood function as computed by the extended Kalman filter, enjoys good finite sample properties. The simulated data for this study have been given similar properties as those in the historical data record 1959–2022. When estimation is actually carried out on the historical data, a statistical model selection procedure has indicated that a forcing equation consisting of a single logarithmic term is adequate for describing the relationship between atmospheric concentrations of CO_2 and the corresponding radiative forcing. The resulting model has been validated using two different methods: first, by showing that the estimated residuals conform the theoretical expectations; second, by showing that the estimated climate variables accurately reproduce the

historical data over the period 1959–2022. We regard (i) Monte Carlo simulation studies for assessing the quality of the estimators, (ii) statistical model selection procedures for informing model specification, and (iii) statistical validations for checking possible model misspecification, as important features of empirical statistical modelling. However, to the best of our knowledge, such statistical methods have not previously been applied to RCMs that model the entire chain from emissions to temperatures, due to the physics-based (deterministic) formulation of these models. Conversely, due to the statistical nature of the Stat-RCM, these analyses can be performed using well-established methodology.

By extracting the latent temperature state using the extended Kalman filter, we have estimated the 2022 long-term global temperature anomaly to be $+1.27^{\circ}\text{C}$ with respect to the 1850–1900 baseline. We also have used the Stat-RCM to project the climate variables until 2100, conditional on a scenario for future CO_2 emissions and radiative forcing from non- CO_2 sources. We have found that in the SSP119 scenario, where emissions are rapidly declining, the 1.5°C Paris upper limit on the global surface temperature anomaly, compared to a 1850–1900 baseline, is not a forgone conclusion. The Stat-RCM estimates a 90% probability that the 1.5°C threshold will be breached by a temperature measurement $T_t^{m,*}$ in the period 2023–2100 under the SSP119 scenario. However, if we consider only the underlying temperature trend, represented by the latent state T_t^m , the Stat-RCM estimates that there is only a 7% probability that the threshold will be breached in the period 2023–2100 under the SSP119 scenario. In the latter case, the uncertainty is epistemic (i.e. stemming from unknown parameters), while, in the former case, aleatoric uncertainty is also included (i.e. uncertainty from internal variability in the climate system, including measurement errors and ENSO effects).

We have focused on estimating the Stat-RCM parameters from the historical data 1959–2022. The main application of RCMs, however, has been as “emulators”, where the RCM is used to emulate the output of large-scale climate models (Nicholls et al., 2020). In future work, we intend to employ the Stat-RCM as an emulator by estimating it using output from large-scale climate models, such as that those from the Coupled Model Intercomparison Project (CMIP; Eyring et al., 2016). This will allow us to employ the statistical methodology illustrated in this paper to output from CMIP models with the aim of complementing the results from existing RCMs, increasingly used in the IPCC reports, with those from the Stat-RCM.

References

- Bacastow, R. B. and C. D. Keeling (1979). Models to predict future atmospheric CO₂ concentrations. In *Workshop on the global effects of carbon dioxide from fossil fuels*, pp. 72–90. US Department of Energy.
- Bennedsen, M., E. Hillebrand, and S. J. Koopman (2023). A multivariate dynamic statistical model of the global carbon budget 1959–2020. *Journal of the Royal Statistical Society Series A: Statistics in Society* 186(1), 20–42.
- Bennedsen, M., E. Hillebrand, and J. Z. Lykke (2023). Global temperature projections from a statistical energy balance model using multiple sources of historical data. *Journal of Climate* 36(19), 6817–6838. Working paper available at <https://arxiv.org/abs/2205.10269>.
- Betts, R. A., S. E. Belcher, L. Hermanson, A. K. Tank, J. A. Lowe, C. D. Jones, C. P. Morice, N. A. Rayner, A. A. Scaife, and P. A. Stott (2023). Approaching 1.5°C: how will we know we’ve reached this crucial warming mark? *Nature* 624, 33–35.
- Brockwell, P. J. and R. A. Davis (1996). *Introduction to time series and forecasting*. Springer New York.
- Cheng, L., K. E. Trenberth, J. Fasullo, T. Boyer, J. Abraham, and J. Zhu (2017). Improved estimates of ocean heat content from 1960 to 2015. *Science Advances* 3(3), e1601545.
- Cummins, D. P., D. B. Stephenson, and P. A. Stott (2020). Optimal estimation of stochastic energy balance model parameters. *Journal of Climate* 33(18), 7909–7926.
- Durbin, J. and S. J. Koopman (2012). *Time series analysis by state space methods*. Number 38. Oxford University Press.
- Durbin, J. and G. S. Watson (1971). Testing for serial correlation in least squares regression. *Biometrika* 58(1), 1 – 19.
- Engle, R. (1988). Autoregressive conditional heteroscedasticity with estimates of the variance of United Kingdom inflation. *Econometrica* 96, 893–920.
- Eyring, V., S. Bony, G. A. Meehl, C. A. Senior, B. Stevens, R. J. Stouffer, and K. E. Taylor (2016). Overview of the Coupled Model Intercomparison Project Phase 6 (CMIP6) experimental design and organization. *Geoscientific Model Development* 9(5), 1937–1958.
- Forster, P., T. Storelvmo, K. Armour, W. Collins, J.-L. Dufresne, D. Frame, D. Lunt, T. Mauritsen, M. Palmer, M. Watanabe, M. Wild, and H. Zhang (2021). The Earth’s energy budget, climate feedbacks, and climate sensitivity. In V. Masson-Delmotte, P. Zhai, A. Pirani, S. Connors, C. Péan, S. Berger, N. Caud, Y. Chen, L. Goldfarb, M. Gomis, M. Huang, K. Leitzell, E. Lonnoy, J. Matthews, T. Maycock, T. Waterfield, O. Yelekçi, R. Yu, and Z. B. (Eds.), *Climate Change 2021: The Physical Science*

- Basis. Contribution of Working Group I to the Sixth Assessment Report of the Intergovernmental Panel on Climate Change.* Cambridge: Cambridge University Press. In Press.
- Friedlingstein, P. (2015). Carbon cycle feedbacks and future climate change. *Philosophical Transactions of the Royal Society A* 373, 20140421.
- Friedlingstein, P., J. L. Dufresne, P. M. Cox, and P. Rayner (2003). How positive is the feedback between climate change and the carbon cycle? *Tellus B: Chemical and Physical Meteorology* 55(2), 692–700.
- Friedlingstein, P., M. O’Sullivan, and et al. (2022). Global Carbon Budget 2022. *Earth System Science Data* 14(11), 4811–4900.
- Fung, I. Y., S. C. Doney, K. Lindsay, and J. John (2005). Evolution of carbon sinks in a changing climate. *Proceedings of the National Academy of Sciences* 102(32), 11201–11206.
- Gregory, J. M. (2000). Vertical heat transports in the ocean and their effect on time-dependent climate change. *Climate Dynamics* 16(7), 501–515.
- Hansen, J., I. Fung, A. Lacis, D. Rind, S. Lebedeff, R. Ruedy, G. Russell, and P. Stone (1988). Global climate changes as forecast by Goddard Institute for Space Studies three-dimensional model. *Journal of Geophysical Research: Atmospheres* 93(D8), 9341–9364.
- Hansen, J. E., M. Sato, A. Lacis, R. Ruedy, I. Tegen, and E. Matthews (1998). Climate forcings in the industrial era. *Proceedings of the National Academy of Sciences* 95(22), 12753.
- Hartin, C. A., P. Patel, A. Schwarber, R. P. Link, and B. P. Bond-Lamberty (2015). A simple object-oriented and open-source model for scientific and policy analyses of the global climate system – Hector v1.0. *Geoscientific Model Development* 8(4), 939–955.
- Haustein, K., M. R. Allen, P. M. Forster, F. E. L. Otto, D. M. Mitchell, H. D. Matthews, and D. J. Frame (2017). A real-time Global Warming Index. *Scientific Reports* 7(1), 15417.
- IPCC (2023). Climate Change 2023 Synthesis Report - Summary for policy makers. Technical report, Intergovernmental Panel on Climate Change (IPCC), https://www.ipcc.ch/report/ar6/syr/downloads/report/IPCC_AR6_SYR_SPM.pdf.
- Jarque, C. M. and A. K. Bera (1987). A test for normality of observations and regression residuals. *International Statistical Review* 2, 163–172.
- Joos, F., M. Bruno, R. Fink, U. Siegenthaler, T. Stocker, C. L. Quéré, and J. L. Sarmiento (1996). An efficient and accurate representation of complex oceanic and biospheric models of anthropogenic carbon uptake. *Tellus* 48B, 397–417.

- Leach, N. J., S. Jenkins, Z. Nicholls, C. J. Smith, J. Lynch, M. Cain, T. Walsh, B. Wu, J. Tsutsui, and M. R. Allen (2021). FaIRv2.0.0: a generalized impulse response model for climate uncertainty and future scenario exploration. *Geoscientific Model Development* 14(5), 3007–3036.
- Lightfoot, H. D. and O. A. Mamer (2014). Calculation of atmospheric radiative forcing (warming effect) of carbon dioxide at any concentration. *Energy & Environment* 25(8), 1439–1454.
- Ljung, G. M. and G. E. P. Box (1978). On a measure of lack of fit in time series models. *Biometrika* 65(2), 297–303.
- Luderer, G., Z. Vrontisi, C. Bertram, O. Y. Edelenbosch, R. C. Pietzcker, J. Rogelj, H. S. De Boer, L. Drouet, J. Emmerling, O. Fricko, S. Fujimori, P. Havlík, G. Iyer, K. Keramidas, A. Kitous, M. Pehl, V. Krey, K. Riahi, B. Saveyn, M. Tavoni, D. P. Van Vuuren, and E. Kriegler (2018). Residual fossil CO₂ emissions in 1.5–2°C pathways. *Nature Climate Change* 8(7), 626–633.
- Masson-Delmotte, V. and P. Zhai (2021). *IPCC Sixth Assessment Report. Climate Change 2021: The Physical Science Basis*. Cambridge University Press.
- Meinshausen, M., N. Meinshausen, W. Hare, S. C. B. Raper, K. Frieler, R. Knutti, D. J. Frame, and M. R. Allen (2009). Greenhouse-gas emission targets for limiting global warming to 2°C. *Nature* 458(7242), 1158–1162.
- Meinshausen, M., Z. R. J. Nicholls, J. Lewis, M. J. Gidden, E. Vogel, M. Freund, U. Beyerle, C. Gessner, A. Nauels, N. Bauer, J. G. Canadell, J. S. Daniel, A. John, P. B. Krummel, G. Luderer, N. Meinshausen, S. A. Montzka, P. J. Rayner, S. Reimann, S. J. Smith, M. van den Berg, G. J. M. Velders, M. K. Vollmer, and R. H. J. Wang (2020). The shared socio-economic pathway (SSP) greenhouse gas concentrations and their extensions to 2500. *Geoscientific Model Development* 13(8), 3571–3605.
- Meinshausen, M., S. C. B. Raper, and T. M. L. Wigley (2011). Emulating coupled atmosphere-ocean and carbon cycle models with a simpler model, MAGICC6 – Part 1: Model description and calibration. *Atmospheric Chemistry and Physics* 11(4), 1417–1456.
- Meinshausen, M., S. J. Smith, K. Calvin, J. S. Daniel, M. L. T. Kainuma, J.-F. Lamarque, K. Matsumoto, S. A. Montzka, S. C. B. Raper, K. Riahi, A. Thomson, G. J. M. Velders, and D. P. P. van Vuuren (2011). The RCP greenhouse gas concentrations and their extensions from 1765 to 2300. *Climatic Change* 109(1), 213.
- Morice, C. P., J. J. Kennedy, N. A. Rayner, J. Winn, E. Hogan, R. Killick, R. Dunn, T. Osborn, P. Jones, and I. Simpson (2020). *An updated assessment of near-surface temperature change from 1850: The HadCRUT5 dataset*. *Journal of Geophysical Research: Atmospheres*.

- Nicholls, Z., M. Meinshausen, and et al. (2021). Reduced complexity model intercomparison project phase 2: Synthesizing earth system knowledge for probabilistic climate projections. *Earth's Future* 9(6), 1–25.
- Nicholls, Z. R. J., M. Meinshausen, J. Lewis, R. Gieseke, D. Dommenges, K. Dorheim, C.-S. Fan, J. S. Fuglestvedt, T. Gasser, U. Golüke, P. Goodwin, C. Hartin, A. P. Hope, E. Kriegler, N. J. Leach, D. Marchegiani, L. A. McBride, Y. Quilcaille, J. Rogelj, R. J. Salawitch, B. H. Samset, M. Sandstad, A. N. Shiklomanov, R. B. Skeie, C. J. Smith, S. Smith, K. Tanaka, J. Tsutsui, and Z. Xie (2020). Reduced Complexity Model Intercomparison Project Phase 1: introduction and evaluation of global-mean temperature response. *Geoscientific Model Development* 13(11), 5175–5190.
- Pretis, F. (2020). Econometric modelling of climate systems: The equivalence of energy balance models and cointegrated vector autoregressions. *Journal of Econometrics* 214(1), 256–273.
- Ramaswami, V. (2001). Chapter 6: Radiative forcing of climate change. Technical report, IPCC.
- Sanderson, B. M., B. C. O'Neill, and C. Tebaldi (2016). What would it take to achieve the Paris temperature targets? *Geophysical Research Letters* 43(13), 7133–7142.
- Schwartz, S. E. (2007). Heat capacity, time constant, and sensitivity of Earth's climate system. *Journal of Geophysical Research* 112(D24), 1–12.
- Schwarz, G. (1978). Estimating the dimension of a model. *The Annals of Statistics* 6(2), 461–464.
- Shi, G. (1992). Radiative forcing and greenhouse effect due to the atmospheric trace gases. *Science in China (Series B)* 35, 217–229.
- Smith, C., D. P. Cummins, H.-B. Fredriksen, Z. Nicholls, M. Meinshausen, M. Allen, S. Jenkins, N. Leach, C. Mathison, and A.-I. Partanen (2024). fair-calibrate v1.4.1: calibration, constraining and validation of the fair simple climate model for reliable future climate projections. *EGUsphere*, 1–36.
- Smith, C., Z. Nicholls, K. Armour, W. Collins, P. Forster, M. Meinshausen, M. Palmer, and M. Watanabe (2021). The earth's energy budget, climate feedbacks, and climate sensitivity supplementary material. In V. Masson-Delmotte, P. Zhai, A. Pirani, S. Connors, C. Péan, S. Berger, N. Caud, Y. Chen, L. Goldfarb, M. Gomis, M. Huang, K. Leitzell, E. Lonnoy, J. Matthews, T. Maycock, T. Waterfield, O. Yelekçi, R. Yu, and Z. B. (Eds.), *Climate Change 2021: The Physical Science Basis. Contribution of Working Group I to the Sixth Assessment Report of the Intergovernmental Panel on Climate Change*. Cambridge: Cambridge University Press. In Press.
- Solomon, S., D. Qin, and M. Manning (2007). *IPCC Fourth Assessment Report. Climate Change 2007: The Physical Science Basis*. Cambridge University Press.

Stocker, T. F. and D. Qin (2013). *IPCC Fifth Assessment Report. Climate Change 2013: The Physical Science Basis*. Cambridge University Press.

Tokarska, K. B. and N. P. Gillett (2018). Cumulative carbon emissions budgets consistent with 1.5 °C global warming. *Nature Climate Change* 8(4), 296–299.

UNFCCC (2015). Adoption of the Paris Agreement, <https://unfccc.int/resource/docs/2015/cop21/eng/109r01.pdf>. Technical report, United Nations Framework Convention on Climate Change.

Zhang, X., Y.-P. Wang, P. Rayner, P. Ciais, K. Huang, Y. Luo, S. Piao, Z. Wang, J. Xia, W. Zhao, X. Zheng, J. Tian, and Y. Zhang (2021). A small climate-amplifying effect of climate-carbon cycle feedback. *Nature Communications* 12, 2952.

A Details of the state space representation of Stat-RCM

Let $y_t = (C_t^*, S_t^{OCN,*}, S_t^{LND,*}, F_t^{CO2,*}, T_t^m, T_t^d, O_t^*)'$ denote the 7×1 vector of observations at time t and $\Delta > 0$ the length of a time step between observations. In Section 3.3 we presented the non-linear state space model of the climate system, given as follows

$$y_t = \mu + Ax_t + \epsilon_t, \quad x_{t+\Delta} = B(x_t) + W_t + R\eta_{t,\Delta},$$

where $x_t = (C_t, S_t^{OCN}, S_t^{LND}, F_t^{CO2}, T_t^m, T_t^d)'$ denotes the 6×1 latent state vector. At time t , there are thus 7 observations, collected in y_t , for 6 states, collected in x_t . The 7×1 vector $\mu = (\mu_C, \mu_L, \mu_O, \mu_F, \mu_m, \mu_d, H_d \cdot \mu_d)'$ contains the intercepts in the measurement equations, and the 7×6 matrix A captures the relations between the observations y_t and the underlying state vector x_t described in Section 3.2,

$$A = \begin{pmatrix} 1 & 0 & 0 & 0 & 0 & 0 \\ 0 & 1 & 0 & 0 & 0 & 0 \\ 0 & 0 & 1 & 0 & 0 & 0 \\ 0 & 0 & 0 & 1 & 0 & 0 \\ 0 & 0 & 0 & 0 & 1 & 0 \\ 0 & 0 & 0 & 0 & 0 & 1 \\ 0 & 0 & 0 & 0 & 0 & H_d \end{pmatrix}.$$

The entries in the 7×1 measurement error vector ϵ_t are modelled as AR(1) processes,

$$\epsilon_{t+\Delta} = \Phi\epsilon_t + \xi_{t,\Delta},$$

with Φ being a 7×7 diagonal matrix given by $\Phi = \text{diag}(\phi_1, \phi_2, \dots, \phi_7)$, with $\phi_i \in (-1, 1)$ for all i , and $\xi_{t,\Delta} \stackrel{iid}{\sim} N(0, \Delta \cdot P)$ with P being the 7×7 matrix

$$P = \begin{pmatrix} \sigma_{\epsilon,C}^2 & 0 & 0 & 0 & 0 & 0 & 0 \\ 0 & \sigma_{\epsilon,OCN}^2 & 0 & 0 & 0 & 0 & 0 \\ 0 & 0 & \sigma_{\epsilon,LND}^2 & 0 & 0 & 0 & 0 \\ 0 & 0 & 0 & \sigma_{\epsilon,F}^2 & 0 & 0 & 0 \\ 0 & 0 & 0 & 0 & \sigma_{\epsilon,m}^2 & 0 & 0 \\ 0 & 0 & 0 & 0 & 0 & \sigma_{\epsilon,d}^2 & \rho\sigma_{\epsilon,d}\sigma_{\epsilon,OHC} \\ 0 & 0 & 0 & 0 & 0 & \rho\sigma_{\epsilon,d}\sigma_{\epsilon,OHC} & \sigma_{\epsilon,OHC}^2 \end{pmatrix},$$

where $\rho \in (-1, 1)$ allows for correlation in the measurement errors of deep ocean temperature $T_t^{d,*}$ and ocean heat content O_t^* , see [Bennedsen et al. \(2023\)](#).

The non-linear 6×1 mapping $B(\cdot)$ represents the state transition equations as described in [Section 3](#),

$$B(x_t) = \begin{pmatrix} C_t \\ b_1 C_t \exp(-c_1 T_t^d) \\ b_2 C_t \exp(-c_2 T_t^d) \\ f_1 \log(C_t + f_2 C_t^2) + f_3 \sqrt{C_t} \\ \left(1 - \frac{\gamma+\lambda}{H_m} \Delta\right) T_t^m + \frac{\gamma\Delta}{H_m} T_t^d \\ \frac{\gamma\Delta}{H_d} T_t^m + \left(1 - \frac{\gamma\Delta}{H_d}\right) T_t^d \end{pmatrix},$$

while the 6×1 vector W_t collects constants and covariates into the state equation,

$$W_t = \begin{pmatrix} C_t - \Delta(b_1 + b_2)C_{1750} + \Delta E_{t+\Delta} \\ -b_1 C_{1750} \\ -b_2 C_{1750} \\ -f_1 \log(C_{1750} + f_2 C_{1750}^2) + f_3 \sqrt{C_{1750}} \\ \frac{\Delta}{H_m} (F_t^{CO2} + F_t^{Ex}) \\ 0 \end{pmatrix}.$$

The 5×1 innovation sequence $\eta_{t,\Delta} \stackrel{iid}{\sim} N(0, \Delta \cdot Q)$ is modelled with a 5×5 diagonal covariance matrix $Q = \text{diag}(\sigma_{\eta,OCN}^2, \sigma_{\eta,LND}^2, \sigma_{\eta,F}^2, \sigma_{\eta,m}^2, \sigma_{\eta,d}^2)$ and the 6×5 matrix R completes the specification for

the state variables,

$$R = \begin{pmatrix} -\Delta & -\Delta & 0 & 0 & 0 \\ 1 & 0 & 0 & 0 & 0 \\ 0 & 1 & 0 & 0 & 0 \\ 0 & 0 & 1 & 0 & 0 \\ 0 & 0 & 0 & 1 & 0 \\ 0 & 0 & 0 & 0 & 1 \end{pmatrix}.$$

Letting $\phi = (\phi_1, \dots, \phi_7)'$, $\sigma_\epsilon^2 = (\sigma_{\epsilon,C}^2, \sigma_{\epsilon,OCN}^2, \sigma_{\epsilon,LND}^2, \sigma_{\epsilon,F}^2, \sigma_{\epsilon,m}^2, \sigma_{\epsilon,d}^2, \sigma_{\epsilon,O}^2)'$, $\sigma_\eta^2 = (\sigma_{\eta,OCN}^2, \sigma_{\eta,LND}^2, \sigma_{\eta,F}^2, \sigma_{\eta,m}^2, \sigma_{\eta,d}^2)$ we arrive at the 37×1 vector θ of unknown parameters, given by

$$\theta = (b_1, b_2, c_1, c_2, f_1, f_2, f_3, \gamma, \lambda, H_m, H_d, \mu_C, \mu_L, \mu_O, \mu_F, \mu_m, \mu_d, \rho, \phi', \sigma'_\epsilon, \sigma'_\eta)'$$

Note that we in our implementation of the Stat-RCM impose several restrictions on the elements in θ , so that the resulting dimension of the parameter vector is smaller than 37. Our preferred specification of the Stat-RCM sets $\mu_C = \mu_L = \mu_O = \mu_F = 0$ and $f_2 = f_3 = 0$, resulting in θ being a 31×1 vector, see Section 5 of the main paper.

In our implementation, we estimate the parameter vector θ by the method of maximum likelihood, using the extended Kalman filter (Durbin and Koopman, 2012, Chapter 10). This procedure requires the Jacobian of the transition function $B(\cdot)$, which is given by

$$\frac{\partial B(x_t)}{\partial x_t'} = \begin{pmatrix} 1 & 0 & 0 & 0 & 0 & 0 \\ b_1 \exp(-c_1 T_t^d) & 0 & 0 & 0 & 0 & -b_1 c_1 C_t \exp(c_1 T_t^d) \\ b_2 \exp(-c_2 T_t^d) & 0 & 0 & 0 & 0 & -b_2 c_2 C_t \exp(c_2 T_t^d) \\ \frac{f_1}{C_t + f_2 C_t^2} (1 + 2f_2 C_t) + \frac{f_3}{2\sqrt{C_t}} & 0 & 0 & 0 & 0 & 0 \\ 0 & 0 & 0 & 0 & \left(1 - \frac{\gamma + \lambda}{H_m} \Delta\right) & \frac{\gamma \Delta}{H_m} \\ 0 & 0 & 0 & 0 & \frac{\gamma \Delta}{H_d} & \left(1 - \frac{\gamma \Delta}{H_d}\right) \end{pmatrix}.$$

B Additional parameter estimates from the Stat-RCM

Section 5.3 of the main paper presents the estimates of the physical parameters of the Stat-RCM when applied to the historical data over the period 1959–2019. The estimated parameters relating to the state (η) and measurement (ϵ) error processes are shown in Tables 5–6. We see that some estimates of the variances of the state disturbances η are estimated to be close to zero, in particular $\hat{\sigma}_{\eta,F}^2, \hat{\sigma}_{\eta,m}^2 \approx 0$. This indicates that for these state variables – corresponding to forcing

Table 5: *Stat-RCM parameter estimates II*

	$\sigma_{\eta,OCN}^2$	$\sigma_{\eta,LND}^2$	$\sigma_{\eta,F}^2$	$\sigma_{\eta,m}^2$	$\sigma_{\eta,d}^2$	$\sigma_{\epsilon,C}^2$	$\sigma_{\epsilon,OCN}^2$	$\sigma_{\epsilon,LND}^2$	$\sigma_{\epsilon,F}^2$	$\sigma_{\epsilon,m}^2$	$\sigma_{\epsilon,d}^2$	$\sigma_{\epsilon,O}^2$	ρ
Estimate:	0.00	0.70	0.00	0.00	0.01	0.45	0.12	0.42	0.01	0.09	0.00	0.04	0.87
Std. Err.:	(0.03)	(0.08)	(0.00)	(0.02)	(0.00)	(0.06)	(0.01)	(0.07)	(0.00)	(0.01)	(0.00)	(0.02)	(0.21)
t-stat:	0.03	9.17	0.00	0.01	11.11	7.20	11.01	5.73	8.97	11.07	1.18	2.71	4.16

Parameter estimates by the maximum likelihood method applied to the 1959–2022 data.

Table 6: *Stat-RCM: Parameter estimates III*

	ϕ_1	ϕ_2	ϕ_3	ϕ_4	ϕ_5	ϕ_6	ϕ_7
Estimate:	0.78	0.56	0.39	0.57	0.15	0.89	0.89
Std. Err.:	(0.08)	(0.11)	(0.21)	(0.15)	(0.13)	(0.07)	(0.07)
t-stat (Asym):	10.00	4.92	1.90	3.80	1.16	12.12	12.11

Parameter estimates by the maximum likelihood method applied to the 1959–2022 data.

from CO₂, $F_t^{CO_2}$, and surface temperature, T_t^m – the internal state dynamics as specified by the three modules of the Stat-RCM are sufficient to capture the evolution of the states. For the remaining state variables, we have $\hat{\sigma}_{\eta,OCN}^2, \hat{\sigma}_{\eta,LND}^2, \hat{\sigma}_{\eta,d}^2 > 0$, indicating that for these states, an additional disturbance term must be included to capture the evolution of the states of the sinks S_t^{OCN} and S_t^{LND} and the deep ocean temperature T_t^d .

It is also worth remarking that $\hat{\rho} = 0.87$, highlighting the close connection between the data on deep ocean temperature ($T_t^{d,*}$) and ocean heat content (O_t^*). We refer to [Bennedson et al. \(2023\)](#) for a more in-depth discussion on the relation between these two time series.